올레일아민과 양쪽성 이온이 그래프트된 폴리아크릴산의 나노입자를 포함하는 폴리우레탄 섬유

아르바나 무하메드*,**,# · 이운형*,# · 남진우* · 티안쿤* · 박주현*,†

*중앙대학교 화학공학과 지능형에너지산업융합학과, **말레이시아 마라 기술대학교 화학공학과

Polyurethane Fibers Bearing Nanoparticles of Polyacrylic Acid Grafted with Oleylamine and Zwitterion

Arbanah Muhammad*,**,#, Woonhyeong Lee*,#, Jinwoo Nam*, Tian Kun*, and Juhyun Park*,†

*Department of Chemical Engineering, Department of Intelligent Energy and Industry,
Chung-Ang University, Seoul 06974, Korea
**Chemical Engineering Studies College of Engineering, Universiti Teknologi MARA,
Cawangan Johor, 81750 Johor, Malaysia

초록: 1-(3-아미노프로필)이미다졸과 1,3-프로판 술톤의 양쪽성 이온이 결합된 신규 유기고분자가 합성되었고 이를 기반으로 나노입자를 제조하였다. 나노입자는 폴리우레탄 섬유에 나노필러로서 역할을 하여 기계적 물성을 향상시키는 동시에 섬유 표면에 위치하여 표면특성을 변화시키는 역할을 하였다. 폴리아크릴산(polyacrylic acid, PAA)에 그래프트 반응을 통해 소수성 올레일아민(oleylamine, OA)과 양쪽성이온을 부착시킴으로써 그래프트 공중합체(PAA-*g*-OA(양쪽성 이온))을 합성하였다. 그 후, 마이크로에멀젼 방법을 사용하여 나노입자를 제조하고 습식 방사 공정을 통해 폴리우레탄(PU) 섬유에 분포시켰다. 결과적인 PU@PAA-*g*-OA(양성 이온)의 신축성 섬유 구조는 높은 파단 신율(600%)을 구현하였고 섬유의 표면특성을 소수성에서 친수성으로 개질시켰다. 고분자 복합체 개발에서 기능성 고분자 나노입자를 활용하는 본 연구의 결과는 섬유 응용 분야에서 향상된 기계적 특성 및 개질된 표면특성을 구현하기 위한 새로운 방법을 제시한다.

Abstract: We developed a novel organic polymer using zwitterion from 1-(3-aminopropyl)imidazole and 1,3-propane sultone to fabricate NPs. Zwitterion was added to polyacrylic acid-grafted oleylamine (PAA-*g*-OA) by COOH activation and amidation to produce PAA-*g*-OA (zwitterion). Thereafter, the NPs were prepared using microemulsion methods and distributed in the polyurethane (PU) fibers via a wet-spinning process. The stretchable fiber structure of PU@PAA-*g*-OA (zwitterion) was demonstrated by the high elongation at break (600%). Also, the hydrophobic surface properties of fibers were modified to hydrophilic ones. These results suggest a novel approach that uses functional polymer nanoparticles to alter surface chemistry and enhance mechanical characteristics in textile applications.

Keywords: amphiphilic nanoparticle, zwitterion, antimicrobial fiber, polyurethane, durability.

Introduction

Typically, microbial infections bind to textiles in an undesirable way, leading to unpleasant odors, color degradation, cross-infection, disease transmission, allergic reaction, and textile deterioration. Owing to their ability to manipulate light, bacteria can quickly destroy textile materials, develop stains, and alter their original color.[1] Sweat promotes the growth of odor-causing bacteria and fungi on fabrics. *Staphylococcus aureus* (*S. aureus*) bacteria are common skin colonizers; they thrive on sweat nutrients and the resultant soil, producing 3-methyl-2-hexonic acid, the compound responsible for body odor in humans. *Escherichia coli* (*E.coli*) bacterium is widely distributed in the environment and can enter the human body through contaminated foods and drinks, causing metabolic illnesses and allergies.[2] As a result of these issues, the antimicrobial features of textiles are important in a wide variety of

#A. Muhammad and W. Lee equally contributed to this work.
†To whom correspondence should be addressed.
jpark@cau.ac.kr, ORCID 0000-0003-1300-5743

applications such as filter surfaces, healthcare items, workwear, domestic goods, sportswear, and personal protection items, including masks, gowns, and disposable bed linens.[3,4]

Natural fibers, such as cotton, have structural features that easily attract bacteria, making them easily degradable.[5] Fibers must possess qualities such as processability, biocompatibility, durability, and stability to be used as textile materials.[6] Synthetic fibers, including nylon, polyamide, polyester, and polyurethane (PU), are also excellent options for fiber fabrication. PU fiber has desirable characteristics that make it an excellent material for apparel. PU polymer solution has excellent tensile and abrasion resistance, is easily spinnable[7] and is flexible.[8] Its structural properties enable it to blend easily with antimicrobial agents, including the amide group that attaches the antimicrobial agent from the inorganic metal ion by complexation.[9,10] Additionally, they blend with hydrophobic and hydrophilic segments to provide an effect during antimicrobial action.[11] To develop into a textile material, however, fibers should have comfort features, such as flexibility and mechanical strength, besides their antimicrobial effect, which still need further development.

In this study, we introduce an antibacterial agent into polymeric nanoparticles (NPs) and use NPs as a nanofillers in the matrix of PU fibers to enhance mechanical properties of the resulting fibers. Choosing the right antimicrobial agents is crucial in developing effective antimicrobial textiles. Previous studies revealed that antibiotics, metal oxides,[12-14] inorganic components,[15] and natural ingredients,[16] have been used as antimicrobial agents in the PU polymer matrix. However, their preparation has the limitations of toxicity to humans and the environment, agglomeration, particle instability, leaching during laundry, poor adherence to fabrics, and a minor reduction in mechanical properties.[17] Alternatively, organic polymers can be used as NPs for developing antimicrobial agents. NPs can provide effective microbial removal with high efficiency, low chemical dosage, and a high surface area-to-volume ratio. A zwitterion is a potential antimicrobial agent that can be prepared using anionic (sulfonate and carbonate) and cationic (quaternary ammonium and imidazolium) groups.[18] It can also be combined with other functional groups to meet desired characteristics. Owing to its neutral charge and pH-dependent charge density, it is classified as a unique substance and can be distinguished from amphiphilic polymers.[19] Its surface charge makes it typically polar and highly hydrophilic, which results in a strong and stable hydration layer. Thus, it is widely used in the preparation of biocompatible and biofouling materials, including membranes[20] and thin films.[21,22] Zwitterion has high bacteriostatic antimicrobial properties because of its hydrophilicity. However, a major drawback that limits its application is the antimicrobial capacity to be retained on the fiber surface preserving or enhancing the mechanical properties of fibers. To resolve this issue, PU fibers were fabricated by incorporating NPs prepared from a newly synthesized polyacrylic acid grafted with oleylamine (OA) and a zwitter ion (PAA-*g*-OA (zwitterion)). It is expected that resulting PU fibers show the strongly enhanced mechanical properties due to the effect of NP fillers and modify the surface characteristics of the fibers because of NPs distributed on surfaces.

Experimental

Materials. PAA, OA (M_W: 267.5 g/mol), 1-(3-aminopropyl)imidazole, (APIM) = (M_W: 125.17 g/mol, 1.049 g/mL), 1,3-propane sultone (MW: 122.14 g/mol, 1.392 g/mL), N,N'-Dicyclohexylcarbodiimide (DCC) (M_W: 206.33 g/mol), dichloromethane (DCM), PU, N,N-dimethylformamide (DMF, 99.8%), chloroform (Ch_3Cl), ethanol (EtOH, anhydrous), methanol, sodium hydroxide (NaOH), and hydrochloric acid (HCl) were used in this study. All chemicals and reagents were of analytical grade, purchased from Sigma–Aldrich Korea, and used without further purification. Ultrapure deionized (DI) water obtained from a Mili-Q system was used to prepare all the solutions.

Graft Copolymer Synthesis. A three-step, PAA-based preparation process was introduced to synthesize the NPs. Zwitterion was first prepared using a facile one-step quaternization reaction under mild conditions. Simultaneously, the PAA-*g*-OA polymer was synthesized by carboxylic group (COOH) activation with DCC coupling before reacting with OA (only one-third of the COOH group was used). The remaining COOH group was then used in the final stage to continue the reaction with zwitterion using the same method to produce PAA-*g*-OA (zwitterion).

To prepare zwitterion (also known as (3-aminopropyl)imidazole) propane sultone), APIM (6.3 g, 50 mmol) and 1,4-propane sultone (6.1 g, 50 mmol) were mixed in EtOH (25 mL). Instantly, a clear, colorless solution, which gradually turned turbid as the reaction progresses, was formed. For 12 h, the mixture was stirred with a 1:1 molar ratio of APIM to sultone. After filtering out any potential unreacted starting material and washing with cold EtOH, a white suspension was finally produced. To obtain a solid product, cold EtOH extraction was carried out by maintaining the sample and EtOH at H_2O: EtOH
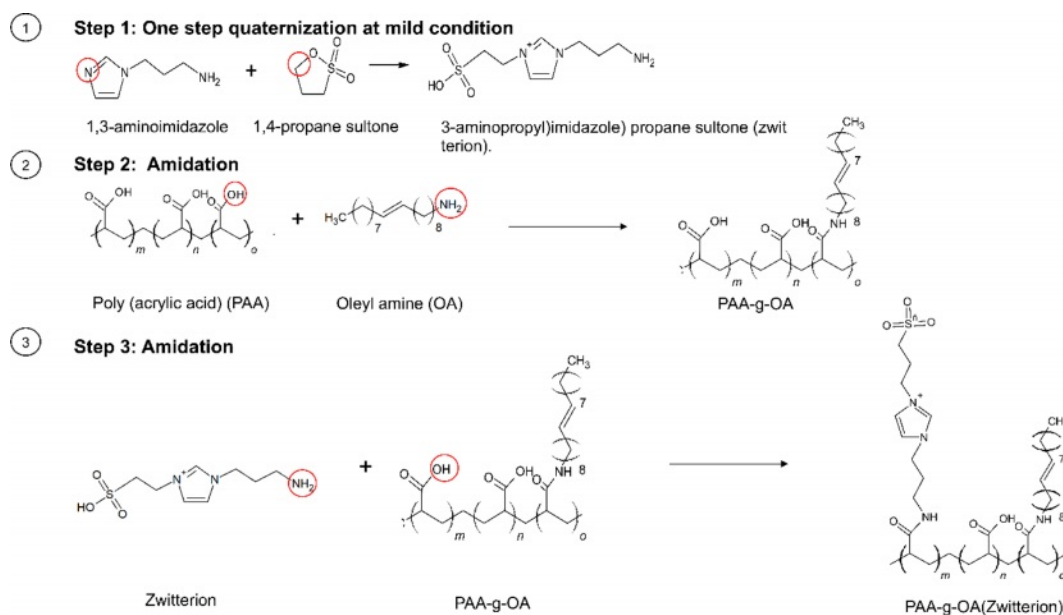
Scheme 1. The three-step synthesis of PAA-*g*-OA(zwitterion).

= 1:10 at a low temperature of -20 ℃. When solid precipitation started to form, the product was filtered, purified, and vacuum-dried.

To prepare PAA-g-OA, 0.9 g of PAA (0.9 g; 12.5 mmol) and DCC (1.56 g; 1.25 mmol) were mixed with 10 mL of DMF and transferred into a round-bottom flask. Then, OA (1.2 mL, 3.6 mmol) was added dropwise into the reaction flask. Thereafter, the mixture was stirred for 16 h. The resulting oily product was washed with DI water after being precipitated with an acidic HCl solution (50 mL; 0.5 M). Centrifugation was used to separate the precipitate, which was then redissolved in 3 mL of methanol before being mixed with 20 mL of 0.5 M HCl. To precipitate the polymer, the final product was dissolved in chloroform (5 mL) and rewashed with HCl (10 mL, 1.0 M) (chloroform: HCl = 1:2). The solution formed two layers, with the bottom being a sticky yellow layer containing the finished product. After being collected, the organic white solid was dried over anhydrous Na$_2$SO$_4$, washed three times with DI water, and mildly stirred for complete precipitation. To eliminate unreacted PAA, the precipitate was centrifuged (8000 rpm, 15 min), and a purified powder was obtained after three rounds of purification.

The COOH group of the synthesized PAA-*g*-OA was activated using DCC to produce PAA-*g*-OA (zwitterion). To eliminate oxygen from the reaction system, the reaction was performed with nitrogen purging for 30 min before proceeding with continuous stirring for 24 h. A bleached yellow pre-

cipitate was formed after zwitterion was added. Diethyl ether and toluene were used to wash the product to eliminate any excess or unreacted polymer; this washing was repeated three times. The product was subsequently decanted to separate the solvent, centrifuged (13500 rpm, 5 min), and dried into powder overnight under a vacuum. The yellow powder zwitterion salt produced by the synthesis had a 95% yield.

Nanoparticle preparation. The PAA-*g*-OA (zwitterion) powder was completely dissolved in chloroform. Thereafter, a small drop was added into the non-solvent, DMF with a ratio of solvent to non-solvent at 1:5 using a 100 µL micropipette. During the dispersion of the polymer NPs, the solution was subjected to ultrasonication for 2 h to break up larger particles and accomplish uniform dispersion.

PU Fiber and Film Fabrication. The PAA-*g*-OA (zwitterion) emulsion solution in DMF and the PU pellet (15 wt%) were combined using stirring at 70 ℃ for 3 h to prepare the PU@ PAA-*g*-OA (zwitterion) solution. Subsequently, the polymer solution was loaded into a plastic syringe equipped with a needle (Do:18 ug) and allowed to sit to remove bubbles. The solution in the syringe was attached to wet spinning equipment and extruded into a water bath to create a precipitated fiber from the solvent exchange. Since water and DMF are highly miscible, a solvent exchange is possible. Also, since DI water is a poor solvent for PU, a precipitate appeared immediately. The PU@PAA-*g*-OA fiber preparation underwent the same preparation procedure. A coagulation bath water solution was prepared at pH

3, 7, and 10 to evaluate the effect of pH on the uniform dispersion of NPs in the fiber. The fiber was allowed to soak for one hour, rinsed with DI water, and then slowly dried at room temperature to ensure complete solvent exchange. The concentrations of the PAA-*g*-OA (zwitterion) NPs were varied at 3, 4, 5, 6, and 7 wt% to evaluate their effect on the fiber characteristics. At the same time, a 5 mL glass petri dish was used to prepare the PAA-*g*-OA (zwitterion) film, which had a 5 cm diameter and a 10 mm thickness. To increase the durability of the NPs on the PU fiber surface, photo-crosslinking was performed by adding Irgacure 2959 (5.887 mmol) to the blending solution. The water-soaked fiber was exposed to a UV lamp for 15 min at a wavelength of 365 nm, and the specific distance between the light and the fiber was set as 3 cm.

Characterization. The nuclear magnetic resonance spectrum (NMR) 300 MHz (Bruker DRX-500 FT-NMR) was used to validate the synthesis of the zwitterion polymer with PAA-*g*-OA. To evaluate structural chemical functional groups of synthesized NPs and fiber, attenuated total reflectance–Fourier transform infrared spectroscopy (ATR-FTIR) was performed with a 4.0 cm^{-1} resolution at a wavenumber range of 1200 to 650 cm^{-1} and an average of 48 scans. The NP and fiber morphology were evaluated using field emission–scanning electron microscopy (FE–SEM) at an accelerating voltage of 5 kV, and the sample was Pt-coated for 180 s at 3 mA. FE–SEM–energy dispersive spectroscopy (EDS) was used to assess the element mapping and distribution of the NPs in the fiber. The water contact angle (WCA) on the film surface was measured using a goniometer, with the film sample. The water droplet was analyzed using a shape analyzer (DSA 25E; Kruss Hamburg, Germany). Five different areas of the film were measured, and the average results were collected. UV-visible spectroscopy was used to assess the optical characteristics. The behavior of the qualitative solution (particle size distribution) was analyzed using the Malvern Zetasizer Nano ZS instrument (at fixed scattering), and the hydrodynamic diameter (Dh) was analyzed using the dynamic light scattering (DLS) unit. For elemental analysis, x-ray photoelectron spectroscopy (XPS) (ThermoFisher Scientific, K-alpha^{+}) was used to calculate the chemical composition of the synthesis material, and the atomic composition was established under MgKa excitation radiation (hv = 1253.6 eV) using the binding energy scale. About 100 mg of synthesized PAA-*g*-OA and PAA-*g*-OA (zwitterion) were transferred into a vial and placed in an ultrahigh vacuum to test the kinetic energy of the photoelectrons. The same procedure was used to compare the PU@PAA-*g*-OA and PAA-*g*-

OA (zwitterion) binding on the flat film surface. The depth was measured to be up to 10 nm, which is an ideal depth for surface functionalization. The spectra were obtained using monochromatic (Al K*α*) X-ray beam power (E=40-200 eV) with an area of 400 um. The mechanical properties were measured using the UTM (Inston) at a rate of 65 mm/min at room temperature. The PU@PAA-*g*-OA (zwitterion) and pure PU fibers underwent stress and elongation tests at 2.5 cm, and the average results were recorded.

Results and Discussion

Polymer Synthesis and Structure Characterization. As depicted in Scheme 1, PAA was used as the backbone to prepare PAA-*g*-OA (zwitterion) following the three-step polymer synthesis process. Initially, 1,3 aminoimidazole and 1,4 propane sultone were quaternized in a single step under mild conditions to create zwitterion. Simultaneously, COOH activation of PAA was performed by coupling with DCC to enable the grafting of OA and zwitterion by amidation. During PAA-*g*-OA preparation, PAA was covalently conjugated with OA, and its molar ratio was adjusted in such a way that the remaining part of the COOH could be conjugated with zwitterion. The resulting comb-like branched structure consists of hydrophilic sites (COOH from PAA and SO$_3^-$ from zwitterion), as well as hydrophobic sites from the OA, both of which contributed to the desired final product and the amphiphilic properties of the polymer.

The synthesis of zwitterion at Step 1 was evaluated using the HNMR, as shown in Figure 1(a). The presence of quaternary ammonization, which reduces the electron cloud density of the imidazole ring was confirmed by the synthesis of the zwitterion from quaternization, which exhibited peaks at δ: 7.29, 7.21, and 7.12 ppm. After the addition of the propionic sulfonate chain, the resonance of the proton was red-shifted to δ: 7.14, 6.85, and 6.79 ppm. This indicates that propane sultone was added *via* aminoalkylsiloxane to open the ring. Furthermore, a downfield shift of the quaternized imidazole on the propionic amine side from 3.5 ppm to 4 ppm revealed proton resonances from CH$_2$ directly connected to the quaternized imidazole on the propionic amine. The result was similar to that of other literature.[23] Since the polymer synthesis for PAA-*g*-OA and PAA-*g*-OA (zwitterion) was achieved through amide bonding, a shifted peak for COOH to CONH was observed. The NH$_2$ amide bond (C-NH$_2$) at δ = 3.29 ppm and the alkene double bond at δ = 5.2 ppm, which represent OA peaks, were
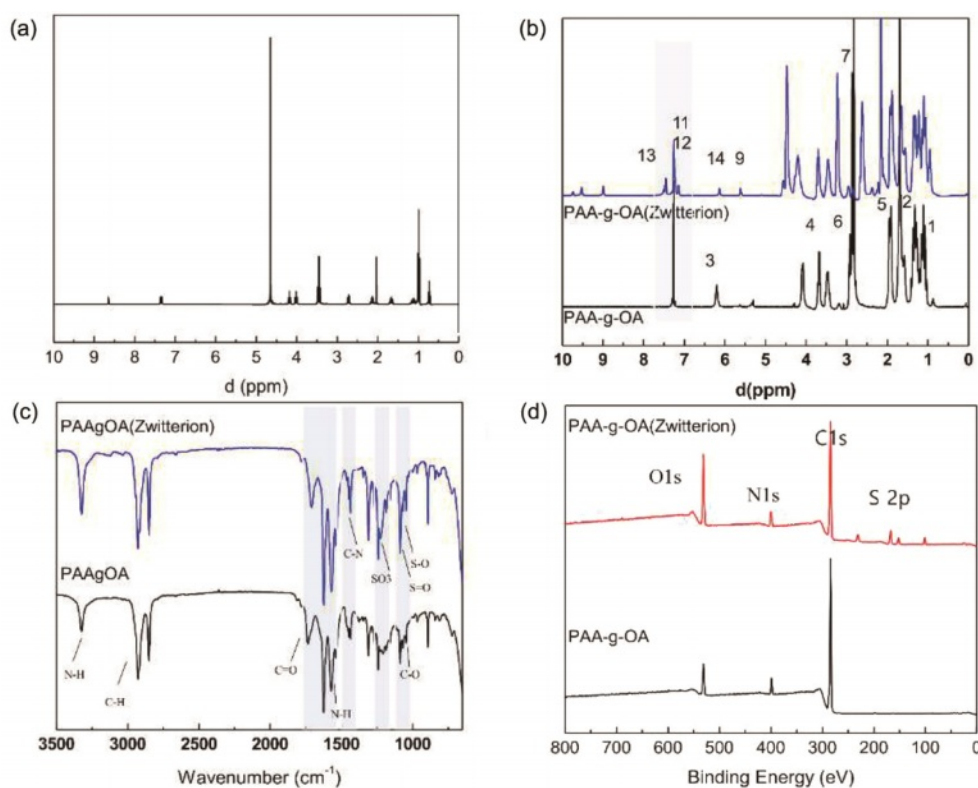
Figure 1. ¹H-NMR spectra of (a) zwitterion; (b) PAA-*g*-OA and PAA-*g*-OAZ; (c) FTIR; (d) fully scanned XPS spectra of PAA-*g*-OA and PAA-*g*-OA (zwitterion).

used to verify the covalent conjugation on the Step 2 PAA-*g*-OA synthesis. Thus, the degree of substitution (DS) can be determined by comparing the peak of the NH₂ and C=OR groups where esterification occurred. The HNMR graph also includes other peaks that label and compare the signal bonding (Figure 1(b)). These findings revealed a monomer conversion/grafting percentage of 52% and a yield of 72%. The presence of three peaks at δ: 7.26, 7.21, and 7.12 ppm, which reflect the phenyl cyclic group from the imidazole after zwitterion grafting with the PAA-*g*-OA, indicates the difference between PAA-*g*-OA and PAA-*g*-OA (zwitterion). There were additional peaks of quaternized imidazole on the propionic amine at $\delta = 4$ ppm, which is absent in PAA-*g*-OA.

The FTIR analysis of the PAA-*g*-OA and PAA-*g*-OA (zwitterion) polymers revealed notable spectra changes (Figure 1(c)). Since both polymers are of the same functional group, the N-H bending peak of amino moieties appeared at 3350-3310 cm⁻¹ and 1650-1580 cm⁻¹. The peak change in the C=O stretching group was due to the amidation reaction in COOH. The C=O peak, which originally appeared at 1726 cm⁻¹, shifted to a lower wavenumber region around 1500-1600 cm⁻¹, indicating the formation of an ionic bond via the electrostatic inter-

action between COOH⁻ and NH⁺ of the co-polymers, OA and zwitterion, to produce CONH. The stretching vibration of C-N in the amide group was ascribed to the additional peaks between 1242 to 1249 cm⁻¹. Additionally, there were additional peaks representing the zwitterion from the imidazole ring (cyclic C=C), ammonium (NH and C=N), and 1,3 propane sultone (SO₃⁻). The aromatic-H peak, which represents the quaternary ammonium group of the imidazole ring, was observed at 954 cm⁻¹. The peaks at 700-900 cm⁻¹ are attributed to the alkene stretching vibration of the imidazole ligand due to the polymerization reaction, which was absent in PAA-*g*-OA. As a result of the stretching vibration of the sulfotone (SO₃⁻) of sulfonic acid, S=O stretching was observed at 1033 cm⁻¹, and C–O bands from the ether groups were observed at 1040 cm⁻¹. This finding is consistent with the molecular structure, demonstrating the successful amidation reaction.

XPS survey scans were conducted for N(1s), C(1s), S(2p), and O(1s) in the NP powder surface to confirm the polymer synthesis. The peaks at 284, 401.5, and 531 eV are assigned to the C1s, N1s, and O1s photoelectrons, respectively. The peak at 401.5 eV corresponded to the N(1s) in the imidazolium ring and oleylamine. The S(2p) scans at 168.38 eV confirmed the

SO_3^- moiety, which is not visible without imidazolium. For PAA-*g*-OA, three C(1s) peaks at 284.81 eV (C-C), 287.12 eV (C-OH), and 288.35 eV (C-O-C) were present. It was found that the C-O-C peak shifted to 288.02 eV in the PAA-*g*-OA (zwitterion) (Figure 1(d)) spectra after the amidation reaction and a new peak appeared at 285.63 eV, representing C-N bonding. The results from the HNMR, FTIR, and XPS analyses reveal inconspicuous changes in the elemental composition of the surface when compared to the control sample, particularly involving the elements N and S.

Nanoparticle Preparation. The characteristics of the colloidal NPs prepared from the microemulsion are presented in Figure 2. Zeta potentials between -100 and 100 mV were obtained for the PAA-*g*-OA NPs and PAA-*g*-OA (zwitterion) NPs dispersed in DMF. In contrast to PAA-*g*-OA that was found to be positive (10.35 mV), PAA-*g*-OA (Zwitterion) present a slightly negative value of -1.134 mV. The charge difference between the two NPs indicates that zwitterion affected the chemical structure, changing the value of the zeta potential due to the isoelectric point of zwitterion, as predicted by the theory. Since the quaternary ammonium group denotes a weaker base compared to the sulfonate group as acid, the sulfobetaine of zwitterion has a strong base and contributes to the negative.

The hydrodynamic size of the PAA-*g*-OA (Zwitterion) NPs was polydispersed, with an average value of 287.1 ± 22.2 nm (Figure 2(b)). This result was expected given that the NP emulsion was prepared using a self-assembly amphiphilic polymer without any surfactant.[24] Thus, their colloidal stability depends on the molecular structure of the polymer, which is influenced by the electrostatic repulsion of $COOH^-$ and the zwitterion surface charge. Particle size distribution strongly affects the optical spectra of colloidal PAA-*g*-OA and PAA-*g*-OA (zwitterion) NPs of the UV-vis absorption (Figure 2(c)). The absorption spectra demonstrate that once zwitterion was added, a small red shift from 270 nm to 277 nm was observed for λ_{max}. This shift proves that zwitterion was conjugated, and the obtained peaks were in acceptable ranges for PAA NPs (CH_3COCH_3) conjugation n-π^*.[25]

The well-defined morphology of the PAA-*g*-OA (zwitterion) NPs is depicted in Figure 2(d). In the surfactant-free NP preparation, the ratio of the hydrophilic and hydrophobic sides depends on the OA and zwitterion moieties. In this study, PAA-*g*-OA had an ellipsoidal structure (<5 μm), while PAA-*g*-OA (zwitterion) had a spherical structure. Since the OA ratio influenced
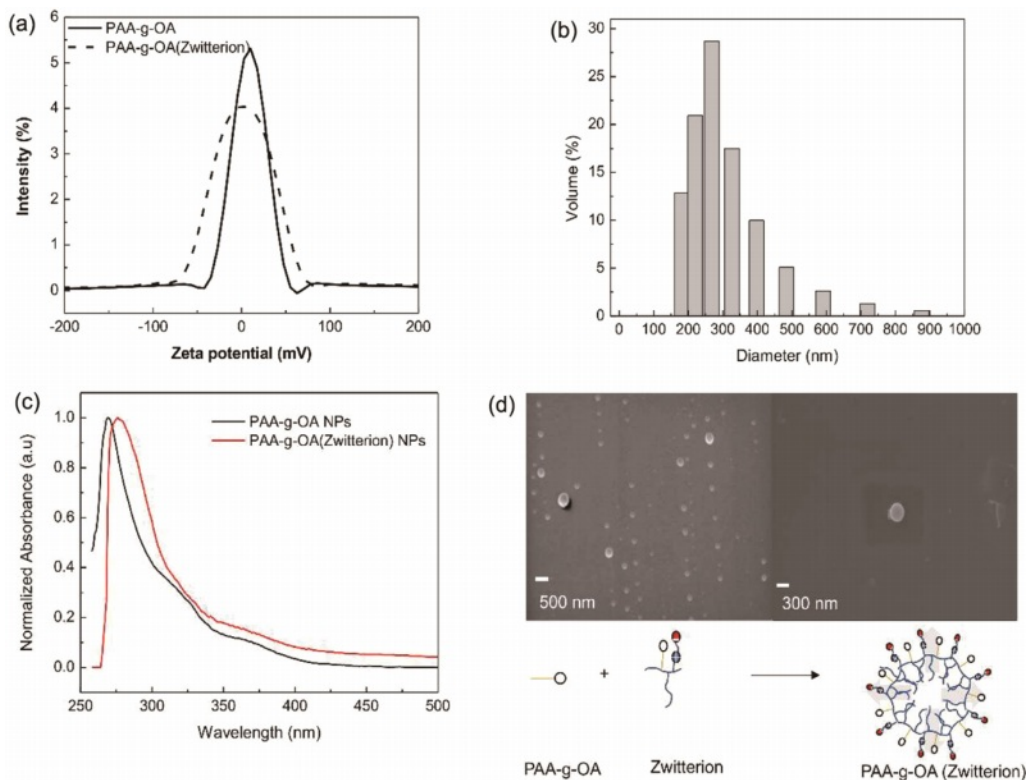

Figure 2. NP characterization: (a) zeta potential; (b) hydrodynamic diameter; (c) optical properties of PAA-*g*-OA (zwitterion) emulsion in the DMF; (d) Micelles structure of the PAA-*g*-OA (zwitterion) NPs.

the NP shape, an ellipsoidal shape was obtained in this preparation at 1:3.3. This formation was due to the NP growth on one side from the long OA alkyl chain. This shape change was expected since the covalent grafting of the polymer precursor made from comb and bottlebrush polymers produced a rod-shaped structure.[26] The theory of a previous study, according to which the rod shape of NPs changes to an elliptical nanocrystal as the ratio of PAA: OA increases from 1:3 to 1:6, provided support for the obtained ellipsoidal shape of PAA-*g*-OA.[27] Meanwhile, after zwitterion was added, a major morphology shifts from ellipsoidal to spherical was observed. This is attributable to the hydrophilic characteristic of zwitterion, which increased the hydrophilic to hydrophobic ratio. Since the hydrophilic part directs the colloidal polymer solution outside and the hydrophobic inside, a spherical shape was created when the solution was dispersed in the non-solvent solution, DMF. This is due to the high polarity of the hydrophilic component of DMF. According to Ofridam *et al*., the amphiphilic and double hydrophilic block copolymers exhibit a micelle structure, which supports the shape change of PAA-*g*-OA (zwitterion) to spherical due to its hydrophilicity.[28] It can be concluded that the surface modification strategies with zwitterionic moieties remarkably improve the colloidal stability and NP morphology.

PU@PAA-*g*-OA (zwitterion) Fiber. The interaction between the PAA-*g*-OA and PAA-*g*-OA (zwitterion) NPs and the PU could be accomplished through hydrogen bonding (Figure 3). The NH group can serve as the proton donor, while the carbonyl/ether oxygen atom can serve as the proton acceptor. To evaluate this interaction, FTIR and XPS investigations were carried out, and all chemical bonds were labeled.

The peak shift or the emergence of new peaks indicates the presence of new bindings (Figure 3(a)). The new peak at 3440 cm^{-1} is associated with the hydrogen-bonded N-H stretching vibration, which became broader with zwitterion addition and showed a new chemical bonding formation. The major peak change was observed at 1735 cm^{-1} and was assigned to stretching-free carboxyl groups, while the shoulder band center near 1706 cm^{-1} was assigned to the stretched hydrogen-bonded carbonyl group, which was stronger than that in the pure PU fiber. Since the functional groups of PU@PAA-*g*-OA and PU@PAA-*g*-OA (zwitterion) are almost identical, the peak changes can only be observed when zwitterion is added from its SO$_3$ position. In PU@PAA-*g*-OA (zwitterion), a new functional group emerged as a sharp new SO$_3$ peak at 1043 cm^{-1} and an amide
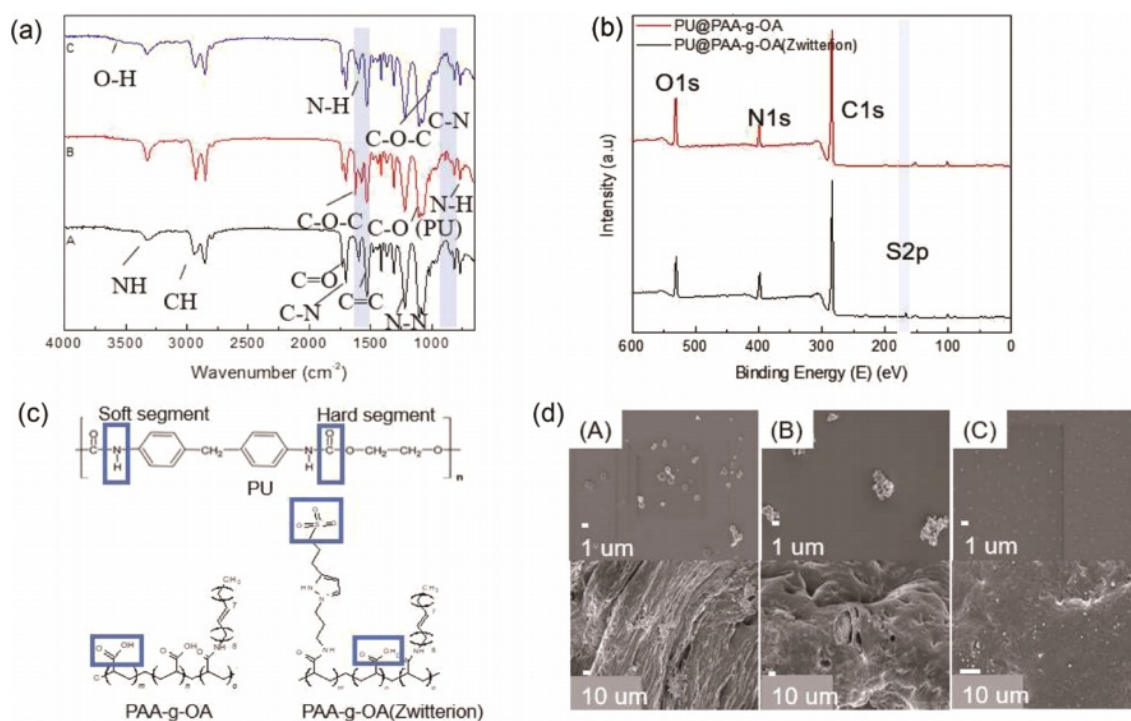

Figure 3. (a) FTIR spectra of the (A) PU fiber, (B) PU@PAA-*g*-OA fiber, and (C) PU@PAA-*g*-OA(Zwitterion) fiber; (b) XPS analysis of the pristine PU fiber and the PU@PAA-*g*-OA(zwitterion) fiber; (c) Schematic molecular structure involvement during hydrogen bonding interaction of PU and the NPs; (d) Morphology analysis of NP dispersion on the PU fiber in the regulated coagulation solution of (A) pH 3, (B) pH 7, and (C) pH 10.

Table 1. Atomic Percentage (%) From the XPS Analysis of the Fiber with Different NPs

Sample	Atomic percentage (at.%)						
	C1s	O1s	N1s	S2p	O/C	N/C	S/C
PU@PAA-*g*-OA	81.03	12.28	6.63	0.0	0.15	0.08	0
PU@PAA-*g*-OA (zwitterion)	77.94	10.46	10.41	1.19	0.13	0.13	0.015

II peak at 1600 cm^{-1} emerged. Our FTIR results exhibited that both the PAA-*g*-OA and PAA-*g*-OA (zwitterion) NPs interact with PU through hydrogen bonding.

XPS spectra of C1s, O1s, N1s, and S2p states in the PU@PAA-*g*-OA and PU@PAA-*g*-OA (Zwitterion) fiber surfaces (Figure 3(b) and S1, and Table 1 and S1) exhibited successful incorporation of NPs into the PU matrix. Especially, the S2p peak at 164 eV verifies the zwitterion in the PU matrix. The atomic peak of S2p representing zwitterion was observed at 1.19%, but this peak was absent in PU@PAA-*g*-OA.

The effect of pH on the uniform dispersion of PAA-*g*-OA (zwitterion) on the PU fiber surface was investigated at different coagulation bath pH levels: pH 3, pH 8, and pH 10 (Figure 3(d)). It is hypothesized that adjusting the coagulation bath pH can influence on the NP distribution on the fiber surface. The results of this study reveal that a change from pH 3 to pH 10 results in a more even distribution of NPs across the fiber surface. The pH of the coagulation bath solution has a major effect on the NP distribution owing to the ionic charge nature of zwitterion. At pH 10, the negatively charged surfaces of the PAA-*g*-OA (zwitterion) NPs preventing the NPs from clumping together by electrostatic repulsion. In contrast, agglomeration occurred at pH 8 and pH 3 because of the abundance of hydrogen ions in the solution, which protonates the zwitterion NPs. This theory is based on a published study that addresses the effect of coagulation buffer pH on polyaniline particle distribution on the polysulfone membrane.[29] As depicted in Figure S2, the FESEM–EDS element mapping of the PU@PAA-*g*-OA (zwitterion) and PU fiber was compared. The elemental mapping revealed a qualitative percentage and uniform distribution of C, O, N, and S on the surface of the PU@PAA-*g*-OA (zwitterion) fiber, as well as the absence of S in the PU fiber.

The surfaces and cross-sections of the PU fibers with various concentrations of the PAA-*g*-OA (zwitterion) NPs are depicted in Figure 4(a) and 4(b). The research was conducted at an NP concentration range of 3% to 7% (w/v). As a result of the induced phase separation, the fiber exhibited a porous cylindrical structure with a mean fiber diameter of 250 ± 5 μm. The pore network emerged once the PU solution precipitated. This was due to the induced phase separation, where solvent exchange appeared since water and DMF are miscible. The NPs were uniformly distributed on the surface and cross-sectional area, demonstrating the good compatibility between the PAA-*g*-OA (zwitterion) NPs and the PU matrix. Under FE–SEM imaging, the smooth cylindrical PU fiber surface was observed to be rough/wrinkled. Once the polymer solution was extruded into a non-solvent solution with small pores, a dense, non-uniform structure emerged on the surface layer of the skin due to the rapid solvent exchange.[30] Because of its hydrophilic properties, zwitterion facilitates solvent exchange on the PU fiber. During the rapid polymer precipitation, large bubbles formed into pores with a finger-like structure rather than a sponge-like shape, as can be seen in the cross-sectional fiber image. Throughout the solvent exchange process, the solvent moved out of the fiber through the pore. Despite the ability of the fiber to retain its porous structure, an increase in the NP concentration induced aggregation. The aggregation was due to the strong hydrogen bonding between the NPs. Since the porosity of fiber depends on the interaction between the solvent and non-solvent solution, the porosity also decreases when the solvent concentration is low. The phase separation process was hindered since the solvent content was reduced at high concentrations. Similar to the findings of a previous investigation, the pores were larger at lower NP concentrations and smaller at higher NP concentrations.[31] Therefore, extruding the fiber beyond 7% (w/v) was challenging due to the high surface tension that resulted in a dense fiber. High concentrations of NPs create an unfavorable situation because the surface tension exceeds the Coulomb force (electrostatic force), making continuous fiber extrusion difficult. Therefore, the test was not extended above 7% (w/v).

Comprehensive mechanical properties of PU@PAA-*g*-OA (zwitterion) were determined by examining their uniaxial tensile tests (Figure 4(c)). The tests were performed on a single fiber strand to assess the impact of different concentrations of NPs to PU on the structural integrity of flexible nanofibers. The findings showed that when compared to that of the pristine PU, the mechanical properties after the NP addition improved. The excellent distribution of NPs in the PU matrix fiber was
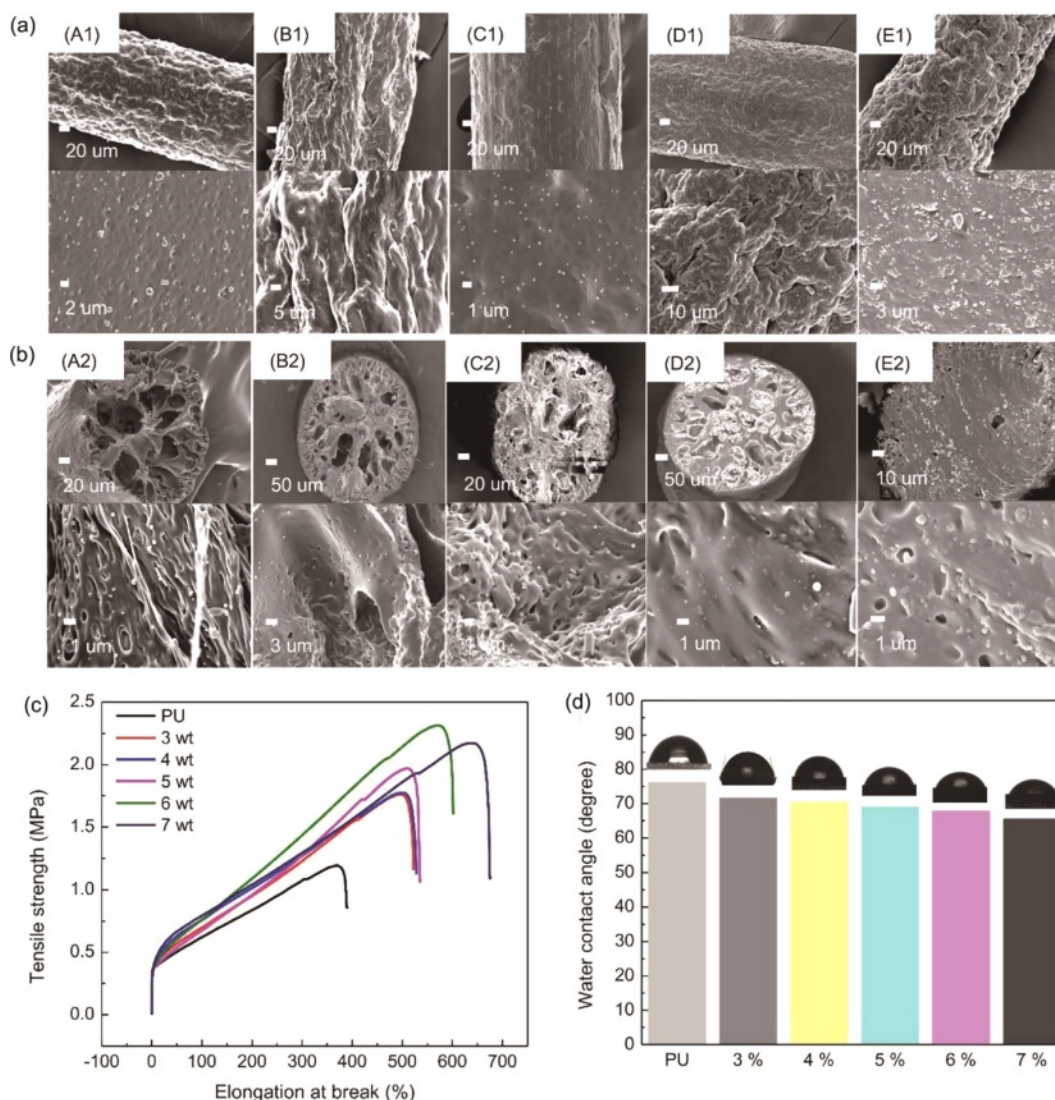
Figure 4. Effect of concentration on the morphology of PU@PAA-*g*-OA (Zwitterion): (a) surface area of (A1) 3%; (B1) 4%; (C1) 5%; (D1) 6%; (E1) 7%; (b) cross-sectional area; (A2) 3%; (B2) 4%; (C2) 5%; (D2) 6%; (E2) 7%; (c) effect of concentration on the PU@PAA-*g*-OA (zwitterion) mechanical properties: (d) variation of water contact angles of PU@PAA-*g*-OA (Zwitterion) relying on NP concentrations.

demonstrated by the increase in tensile strength with NP concentration. When the stress was first applied, the NPs were evenly disseminated within the PU matrix, and the matrix properties were subsequently transferred to the NPs via the interfacial layer. The NPs, which constitute the reinforcement phase structure, supported the dispersing of the stress borne by the matrix to increase the mechanical properties. The low value of stress in comparison to other fiber preparations was due to the wet spinning solution, which produced a porous structure that breaks easily once the stress is introduced.[32] However, the fact that this stress was higher than that of pristine PU demonstrates the effectiveness of NPs in improving mechanical property. More-

over, it is expected that when applied as a fiber mat, rather than as individual strands, it will provide greater mechanical strength. However, the high elongation break shows the strong interfacial adhesion of the NPs to the polymer matrix through covalent bonding, leading to a high crosslinked density between the NH_2 and COOH functional groups. The tensile strength was found to be greatest at 6% (w/v) and increased steadily as the NP concentration increased to 7% (w/v), after which it began to decrease. This is caused by the high concentration of NPs that agglomerates in the fiber and promotes the stress concentration effect. The stress reduction depends on the hydrogen bond of the hard segment, which deteriorates when the

agglomeration appeared. However, the continuous increase in the elongation break at 7% (w/v) to 700% is attributable to the high aspect ratio and Van der Walls attractive interaction between the NPs, as well as their strong interconnected network structure, which maintained the elongation for a longer time. Moreover, the mechanical properties of the PU fiber were divided into two segments; the soft segments, which provide elasticity and can retain their mechanical properties despite an increase in NP concentration, and the hard segment, which is physically crosslinked to increase the tensile strength. The high elongation of PU@PAA-*g*-OA (zwitterion) fiber demonstrates its stretch properties, which are essential for the textile industry's weaving and knitting processes.[30,33,34]

To evaluate the wettability of the PU film with NP addition, the WCA was measured at different PAA-*g*-OA (zwitterion) NP concentrations (Figure 4(d)). The decrease in the WCA below 90° indicates a hydrophilic NP structure. As the NP concentration increased, the WCA reduced to 72.9, 69.9, 67.7, 55.9, and 45.3°. Since the structural properties of zwitterion are hydrophilic owing to its ionic surface charge, it is expected that the hydrophilic property of the film will increase with an increase in PAA-*g*-OA (zwitterion) NP content. By electrostatically inducing hydration, this ionic charge can bind water molecules more strongly. The hydrophilic characteristic of a film shows its ability to absorb and retain water. This property is essential for achieving superior in vitro, wound-healing, and antifouling performances.[35] This finding is consistent with the previous report that demonstrated that zwitterion contributes to the hydrophilicity of polymer composites.[36]

Conclusions

In summary, novel polymer NPs, PAA-*g*-OA (zwitterion), were integrated into wet spinning to create a newly developed PU fiber. Zwitterion was incorporated into the synthesis of the NPs to enhance the hydrophilicity and mechanical property of the fiber. The enhancement was demonstrated using a comparison with PAA-*g*-OA NPs, a manufactured PU fiber without zwitterion. The high elongation at break and improved hydrophilicity of the PU@PAA-*g*-OA (zwitterion) NPs indicate a high potential for textile applications.

Conflict of Interest: The authors declare that there is no conflict of interest.

Supporting Information: Information is available regarding the XPS spectra, binding energies of elements, and EDS spectra of PU bearing NPs. The materials are available *via* the Internet at http://journal.polymer-korea.or.kr.

References

1. Gulati, R.; Sharma, S.; Sharma, R.K. Antimicrobial Textile: Recent Developments and Functional Perspective. *Polym. Bull.* **2022**, 79, 5747-5771.
2. Haindongo, E. H.; Ndakolo, D.; Hedimbi, M.; Vainio, O.; Hakanen, A.; Vuopio, J. Antimicrobial Resistance Prevalence of *Escherichia coli* and *Staphylococcus aureus* amongst Bacteremic Patients in Africa: a Systematic Review, *J. Glob. Antimicrob. Resist.* **2023**, 32, 35-43.
3. Zhang, Y.; Fan, W.; Sun, Y.; Chen, W.; Zhang, Y. Application of Antiviral Materials in Textiles: A review, *Nanotechnol. Rev.* **2021**, 10, 1092-1115.
4. Karim, N.; Afroj, S. S.; Lloyd, K.; Oaten, L. C.; Andreeva, D. V.; Chris, C.; Farmery, A. D.; Kim, I. D.; Novoselov, K. S. Sustainable Personal Protective Clothing for Healthcare Applications: A Review, *ACS Nano* **2020**, 14, 12313-12340.
5. Chen, S.; Chen, S.; Jiang, S.; Xiong, M.; Luo, J.; Tang, J.; Ge, J. Novel Antibacterial Cotton Textiles Finished with Siloxane Sulfopropylbetaine, *ACS Appl. Mater. Interfaces* **2011**, 3, 1154-1162.
6. Park, J. Functional Fibers, Composites and Textiles Utilizing Photothermal and Joule Heating, *Polymers* **2020**, 12, 189.
7. Ahirwar, D.; Telang, A.; Purohit, R.; Namdev, A. A Short Review on Polyurethane Polymer Composite, *Mater. Today. Proc.* **2022**, 62, 3804-3810.
8. Liu, Z.; Li, C.; Zhang, X.; Zhou, B.; Wen, S.; Zhou, Y.; Chen, S.; Jiang, L.; Jerrams, S.; Zhou, F. Biodegradable Polyurethane Fiber-Based Strain Sensor with a Broad Sensing Range and High Sensitivity for Human Motion Monitoring, *ACS Sustain. Chem. Eng.* **2022**, 10, 8788-8798.
9. Sikdar, P.; Dip, T. M.; Dhar, A. K.; Bhattacharjee, M.; Hoque, M. S.; Bin Ali, S. Polyurethane (PU) Based Multifunctional Materials: Emerging Paradigm for Functional Textiles, Smart, and Biomedical Applications, *J. Appl. Polym. Sci.* **2022**, 139, e52832.
10. Xia, Y.; He, L.; Feng, J.; Xu, S.; Yao, L.; Pan, G. Waterproof and Moisture-Permeable Polyurethane Nanofiber Membrane with High Strength, Launderability, and Durable Antimicrobial Properties,

Nanomaterials **2022**, 12, 1813.

11. Mahdavi, H.; Hosseini, F. Fabrication of High-performance Mixed Matrix Blend Membranes Comprising PES and TPU Reinforced with APTS Functionalized-graphene Oxide via VIPS-NIPS Technique for Aqueous Dye Treatment and Antifouling Properties, *J. Taiwan. Inst. Chem. Eng.* **2023**, 142, 104609.

12. Zhang, J.; Li, X.; Guo, J.; Zhou, G.; Xiang, L.; Wang, S.; He, Z. Novel TiO_2/TPU Composite Fiber-based Smart Textiles for Photocatalytic Applications, *Mater. Adv.* **2022**, 3, 1518-1526.

13. Cui, X.; Chen, J.; Wu, W.; Liu, Y.; Li, H.; Xu, Z.; Zhu, Y. Flexible and Breathable All-nanofiber Iontronic Pressure Sensors with Ultraviolet Shielding and Antibacterial Performances for Wearable Electronics, *Nano Energy* **2022**, 95, 107022.

14. Moustafa, H.; Darwish, N. A.; Youssef, A. M. Rational Formulations of Sustainable Polyurethane/chitin/rosin Composites Reinforced with ZnO-doped-SiO_2 Nanoparticles for Green Packaging Applications, *Food Chem.* **2022**, 371, 131193.

15. Erdem Yilmaz, O. Antimicrobial and Gas Adsorption Properties of Electrospun Ferrocene-Polyurethane-Based Nanofibers Containing Silver Nitrate, *Arab. J. Sci. Eng.* **2022**, 48, 389.

16. Gong, D. K.; Zhang, A.; Luo, H.; Shi, Y. D.; Zhang, Y.; Tan, L. Polyhexamethylene Biguanide Hydrochloride Anchored Polymeric Elastic Fibers with Robust Antibacterial Performance, *J. Appl. Polym. Sci.* **2022**, 139, 7.

17. Bhandari, V.; Jose, S.; Badanayak, P.; Sankaran, A.; Anandan, V. Antimicrobial Finishing of Metals, Metal Oxides, and Metal Composites on Textiles: A Systematic Review, *Ind. Eng. Chem. Res.* **2022**, 61, 86.

18. Mi, L.; Jiang, S. Integrated Antimicrobial and Nonfouling Zwitterionic Polymers, *Angew. Chem. Int. Ed.* **2014**, 53, 1746.

19. Wu, A.; Gao, Y.; Zheng, L. Zwitterionic Amphiphiles: Their Aggregation Behavior and Applications, *Green Chem.* **2019**, 21, 4290.

20. Ma, R.; Ji, Y. L.; Guo, Y. S.; Mi, Y. F.; An, Q. F.; Gao, C. J. Fabrication of Antifouling Reverse Osmosis Membranes by Incorporating Zwitterionic Colloids Nanoparticles for Brackish Water Desalination, *Desalination* **2017**, 416, 35.

21. Ji, Y. L.; Qian, W. J.; An, Q. F.; Lee, K. R.; Gao, C. J. Polyelectrolyte Nanoparticles Based Thin-film Nanocomposite (TFN) Membranes for Amino Acids Separation, *J. Ind. Eng. Chem.* **2018**, 66, 209.

22. Ji, Y. L.; An, Q. F.; Weng, X. D.; Hung, W. S.; Lee, K. R.; Gao, C. J. Microstructure and Performance of Zwitterionic Polymeric Nanoparticle/polyamide Thin-film Nanocomposite Membranes for Salts/organics Separation, *J. Membr. Sci.* **2018**, 548, 559.

23. Chen, Y.; Ge, Q. A Bifunctional Zwitterion That Serves as Both a Membrane Modifier and a Draw Solute for Forward Osmosis Wastewater Treatment, *ACS Appl. Mater. Interfaces.* **2019**, 11, 36118.

24. Nakano, T.; Saito, N.; Minami, H. Preparation of Cross-Linked Monodisperse Poly(acrylic acid) Particles by Precipitation Polymerization, *Langmuir* **2020**, 36, 11957.

25. Sun, Z.; Cheng, K.; Wu, F.; Liu, H.; Ma, X.; Su, X.; Liu, Y.; Xia, L.; Cheng, Z. Robust Surface Coating for a fAst, Facile Fluorine-18 Labeling of Iron Oxide Nanoparticles for PET/MR Dual-modality Imaging, *Nanoscale* **2016**, 8, 19644.

26. Nitti, A.; Carfora, R.; Assanelli, G.; Notari, M.; Pasini, D. Single-Chain Polymer Nanoparticles for Addressing Morphologies and Functions at the Nanoscale: A Review, *ACS Appl. Nano Mater.* **2022**, 5, 13985.

27. Lee, S. S.; Zhu, H.; Contreras, E. Q.; Prakash, A.; Puppala, H. L.; Colvin, V. L. High Temperature Decomposition of Cerium Precursors to form Ceria Nanocrystal Libraries for Biological Applications, *Chem. Mater.* **2012**, 24, 424.

28. Ofridam, F.; Tarhini, M.; Lebaz, N.; Gagnière, E.; Tarhini, M.; Lebaz, N. pH-sensitive Polymers: Classification and Some Fine Potential Applications, *Polym. Adv. Technol.* **2021**, 1455.

29. Zhao, S.; Wang, Z.; Wang, J.; Wang, S. The Effect of pH of Coagulation Bath on Tailoring the Morphology and Separation Performance of Polysulfone/polyaniline Ultrafiltration Membrane, *J. Membr. Sci.* **2014**, 469, 316.

30. Lu, Y.; Jiang, J.; Yoon, S.; Kim, K.-S.; Kim, J.-H.; Park, S.; Kim, S.-H.; Piao, L. High-Performance Stretchable Conductive Composite Fibers from Surface-Modified Silver Nanowires and Thermoplastic Polyurethane by Wet Spinning, *ACS Appl. Mater. Interfaces* **2018**, 10, 2093-2104.

31. He, Z.; Byun, J. H.; Zhou, G.; Park, B. J.; Kim, T. H.; Lee, T. S. B.; Yi, J. W.; Um, M. K.; Chou, T. W. Effect of MWCNT Content on the Mechanical and Strain-sensing Performance of Thermoplastic Polyurethane Composite Fibers, *Carbon.* **2019**, 146, 701.

32. Abzan, N.; Kharaziha, M.; Labbaf, S.; Saeidi, N. Modulation of the Mechanical, Physical and Chemical Properties of Polyvinylidene Fluoride Scaffold via Non-solvent Induced Phase Separation Process for Nerve Tissue Engineering Applications, *Eur. Polym. J.* **2018**, 104, 115.

33. Kwak, S. S.; Kim, H.; Seung, W.; Kim, J.; Hinchet, R.; Kim, S. W. Fully Stretchable Textile Triboelectric Nanogenerator with Knitted Fabric Structures, *ACS Nano* **2017**, 11, 10733.

34. Yu, L.; Yeo, J. C.; Soon, R. H.; Yeo, T.; Lee, H. H.; Lim, C. T. Highly Stretchable, Weavable, and Washable Piezoresistive Microfiber Sensors, *ACS Appl. Mater. Interfaces.* **2018**, 10, 12773.

35. Guo, F. C.; Chen, C. Y. Zwitterionic Core-Sheath Nanofibers in Antibacterial Photodynamic Therapy, *ACS Appl. Polym. Mat.* **2022**, 4, 4576.

36. Blackman, L. D.; Gunatillake, P. A.; Cass, P.; Locock, K. E. S. An Introduction to Zwitterionic Polymer Behavior and Applications in Solution and at Surfaces, *Chem. Soc. Rev.* **2019**, 48, 757.